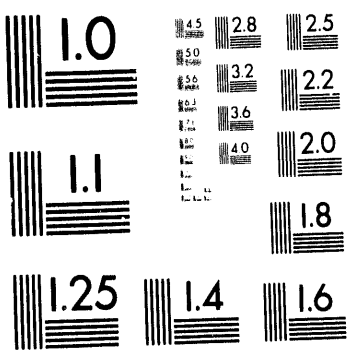
1.0
1.1
1.25
1.4
1.6
1.8
2.0
2.2
2.5
2.8
3.2
3.6
4.0
4.5
5.0
5.6

1 of 1

UCRL-JC-112452
PREPRINT

Studies on Reducing the Scale of a Double Focusing Mass Spectrometer

D. M. Chambers
H. R. Gregg
B. D. Andresen

This paper was prepared for submittal to the
American Society of Mass Spectrometry
San Francisco, Ca
May 30 thru June 4, 1993

May 1993

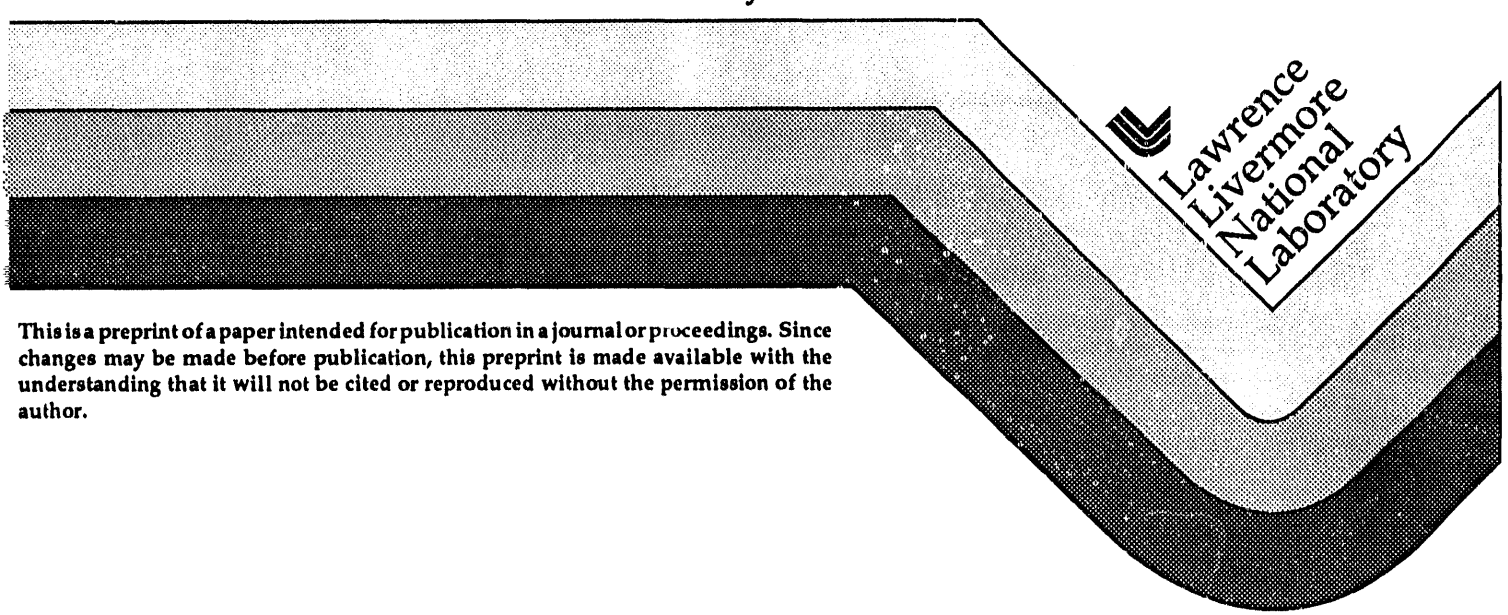

Studies on Reducing the Scale of a Double Focusing Mass Spectrometer

David M. Chambers, Hugh R. Gregg, Brian D. Andresen
Lawrence Livermore National Laboratory
P.O. Box 808, Livermore CA 94551

Introduction

Several groups have developed miniaturized sector mass spectrometers with the goal of remote sensing in confined spaces or portability [1–3]. However, these achievements have been overshadowed by more successful development of man-portable quadrupole and ion trap mass spectrometers. Despite these accomplishments the development of a reduced-scale sector mass spectrometer remains attractive as a potentially low-cost, robust instrument requiring very simple electronics and low power. Previous studies on miniaturizing sector instruments include the use of a Mattauch-Herzog design for a portable mass spectrograph weighing less than 10 kg [1]. Other work has included the use of a Nier-Johnson design in spacecraft-mountable gas chromatography mass spectrometers for the Viking spacecraft [2] as well as miniature sector-based MS/MS instrument [3]. Although theory for designing an optimized system with high resolution and mass accuracy is well understood, such specifications have not yet been achieved in a miniaturized instrument. These shortcomings are often the result of compromises made to fulfill the low-cost, simple and robust instrument objective.

To proceed further toward the development of a miniaturized sector mass spectrometer, experiments were conducted to understand and optimize a practical, yet nonideal instrument configuration. The sector mass spectrometer studied in this work is similar to the ones developed for the Viking project, but was further modified to be low cost, simple and robust. Characteristics of this instrument that highlight its simplicity include the use of a modified Varian leak detector ion source, source ion optics that use require one extraction voltage, and an unshunted fixed nonhomogeneous magnetic sector. The effects of these design simplifications on ion trajectory were studied by manipulating the ion beam along with the magnetic sector position. This latter feature served as an aid to study ion focusing amidst fringing fields as well as nonhomogeneous forces and permitted empirical realignment of the instrument.

Experimental

The mass spectrometer design employs a Nier-Johnson configuration with a 90° angular deflection through each the electric and magnetic sector. The arrangement of the instrument studied has been described by Andresen *et al.* [4] and is shown in Fig 1. Dimensions are detailed in Table 1.

[1] M.P. Sinha and A.D. Tomassian, Rev. Sci. Instrum. **62**, 2618 (1991).
[2] D.R. Rushneck *et al.*, Rev. Sci. Instrum. **49**, 817 (1987).
[3] A. Baes, B. Eckenrode, and R. Drew 38th ASMS Conference on Mass Spectrometry and Allied Topics; Nashville, TN; May 19–24, 1991; p. 164.
[4] B.D. Andresen, J.D. Eckels, J.F. Kimmons, W.H. Martin, D.W. Myers and R.F. Keville, U.S. Patent 5,153,433 (1992).

The source region was maintained at the same pressure as the mass analyzer chamber. The ion source filament assembly was from a Varian leak detector (PN 981-82850-301) equipped with three sets of optics and was coupled to an extraction lens stack. The filament optic potentials, filament current and accelerating potential were driven with a master electronic control unit (MEC-4, Premier American Technologies). Ion extraction from the source was accomplished by applying a potential from a separate floating DC power supply (Harrison 6522A) across the lens stack. The electrostatic energy analyzer (ESA), which was a cylindrical condenser of 1.905 cm in height, was powered by another floating DC supply constructed in house. The object slit before the ESA, S_1, bisected the 2.5-mm diameter ion beam emanating from the source and was centered with respect to the ESA. The ESA fringing fields were shunted where the effective field boundary was calculated to extend 1.57 mm beyond the ESA. The magnetic sector consisted of two 5.08-cm square neodymium iron boron magnets with pointed tips that were separated by 2.54 mm. The residual flux density for each magnet was approximately 12.1 kG that could vary up to 10% across the surface. Although the calculated magnetic flux density at the center of the magnetic sector, B_o, was 8226 G the measured value was approximately 7630 G. No fringing field shunts were used to limit the effective field boundary.

The mass range of the current instrument configuration extended from 0 to approximately 230 amu with resolution at m/Δm of over 300. The accelerating potential was varied from a factor of 4.446 to 4.611 of the accelerating voltage in these experiments. The accelerating potential could be scanned linearly from 1071 to 0V.

Results and Discussion

Optimal signal and resolution could only be achieved by deflecting the ion beam from the axis (ESA center radius, r_e) toward the inner condenser, thus decreasing r_m and shortening the ion path length. Inward deflection was performed by decreasing the ratio of accelerating to ESA potential. Although this action complicates ion trajectory by accelerating the ion beam as well as the angle of trajectory out of the ESA, optimal resolution and signal could be achieved empirically by fine-tuning the magnet sector position. Departure from the optic axis is plotted in Fig. 2 along with the corresponding entrance depth into the magnetic sector. The position at which ions were expected to enter the magnetic sector was determined from the initial trajectory of the ion beam leaving the ESA. Linear extrapolation of the results in Fig. 2 to zero deflection yields a corresponding magnetic sector entrance depth of 3.468 cm, which was beyond the translation range of the magnetic sector assembly. At a fixed l_{e1}, r_e, r_m and l_{m2}, the experimental system exhibits an $l_{e2}+l_{m1}$, 5.75 mm shorter than what first-order theory predicts (i.e., 9.982 cm). Xenon doubly charged isotope signals that correspond to the least and greatest amount of ion deflection are displayed as part of Fig. 2. The best resolution was achieved when ion deflection was the largest.

Shown in Fig. 3 is the calculated flux density distribution as a function of distance. Once outside the magnet boundary the flux drops quickly. For example, at 5 mm away from the magnet the flux density drops off to 10% of B_o. However, at large distances a relatively weak field persists out to the ESA shunt. This fringing field can remain virtually negligible as long as ions are maintained at a relatively high kinetic energy. To the lowest order the effective field boundary for the magnet can be approximated at the magnet boundary itself.

The magnet position could be moved nearly 5 mm perpendicular to the incoming ion beam with little change in resolution and signal. This response is shown in Fig. 4 for the Xe doubly charged ions and is attributed to the magnetic sector geometry and movement direction. In the simplest case where the ion entrance depth into the magnet, **a**, is nearly

equal to the ion exit depth, **h**, (see Fig. 5) there will be a negligible change in the ion radius, r_m, by

$$h = \sqrt{r_m \times 2a - a^2}$$

Plotted in Fig. 6 is the effect of changing **a** on **h** where r_m is 3.744 cm, which is the radius that corresponds to the greatest amount of ion beam deflection out of the ESA shown in Fig. 2. The results plotted in Fig. 6 were calculated by modifying the above equation to take into account the ion beam exit angle required to reach the detector slit, S_3, given **a**. For values of **a** less than 3.823 cm the ion beam will exit the magnetic sector left of the detector and must be angled toward the detector. Also plotted in Fig. 6 are the ion beam entrance depths corresponding to the data in Fig. 4. Ideally, the optimum operation range should correspond to the top of the curve, nevertheless, **h** varies only slightly with **a** over the experimental region studied. As a result, the most significant change in ion path as the magnet is moved is the distance l_{m2}.

Shown in Fig. 7 are mass calibration plots for the xenon doubly charged ion isotopes at different r_m values. From the accelerating potentials and r_m values, which were calculated on the basis of **a** and the location of the detector slit (i.e., S_3), the experimental magnetic flux density ranges from 7397 to 7231 G. These values are lower than the measured value in the center of the magnet of 7630 G.

Conclusion

Deviations from first-order theory are believed to be, in part, associated with simplifications made to the instrument design that include using an unshunted nonhomogeneous magnetic sector. To achieve ion focusing with zero ion deflection out of the ESA the ion path length needs to be shortened with respect to first-order theory. Future modifications will include decreasing l_{m2} as well as the magnetic sector ion exit depth (i.e., move the detector assembly left). These modification should allow the ion beam to travel horizontally from the ESA to the magnetic sector and vertically from the magnetic sector to the detector.

The mass spectrometer instrument presented here is highlighted by its inexpensive and simple analyzer and electronics design. However, the mass range is restricted by the upper accelerating potential needed for the detection of low masses and suitable resolution at higher masses. For this instrument, baseline resolution was achieved for ions with kinetic energy on the order of 500 eV, which corresponds to an m/z of 70. A significant drop in resolution was seen at increasingly higher m/z values and is attributed to electronic ripple as well as nonhomogeneous and fringing field effects. One possible approach to shift the analysis range of the mass analyzer to higher masses would be to increase r_m. This trend is exemplified in Fig. 7 where accelerating potentials for a paricular m/z ion increase with r_m.

Work performed under the auspices of the U.S. Department of Energy by the Lawrence Livermore National Laboratory under contract W-7405-ENG-48.

Table 1

Curvature through ESA	r_e	4.699 cm
ESA Gap	G_e	5.03 mm
Angular Deflection in ESA	ϕ_e	90°
Curvature through Magnet	r_{m1}	3.823 cm
Angular Deflection in Magnet	ϕ_m	90°
Object Slit before ESA	S_1	25 μm
ESA Object Length	l_{e1}	6.71 mm
ESA Image Length	l_{e2}	2.920 cm
Magnet Object Length	l_{m1}	7.061 cm
Magnet Image Length	l_{m2}	2.070 cm
Image Slit after Magnet	S_3	38 μm

Fig 1

Reduced-Scale Sector Mass Spectrometer

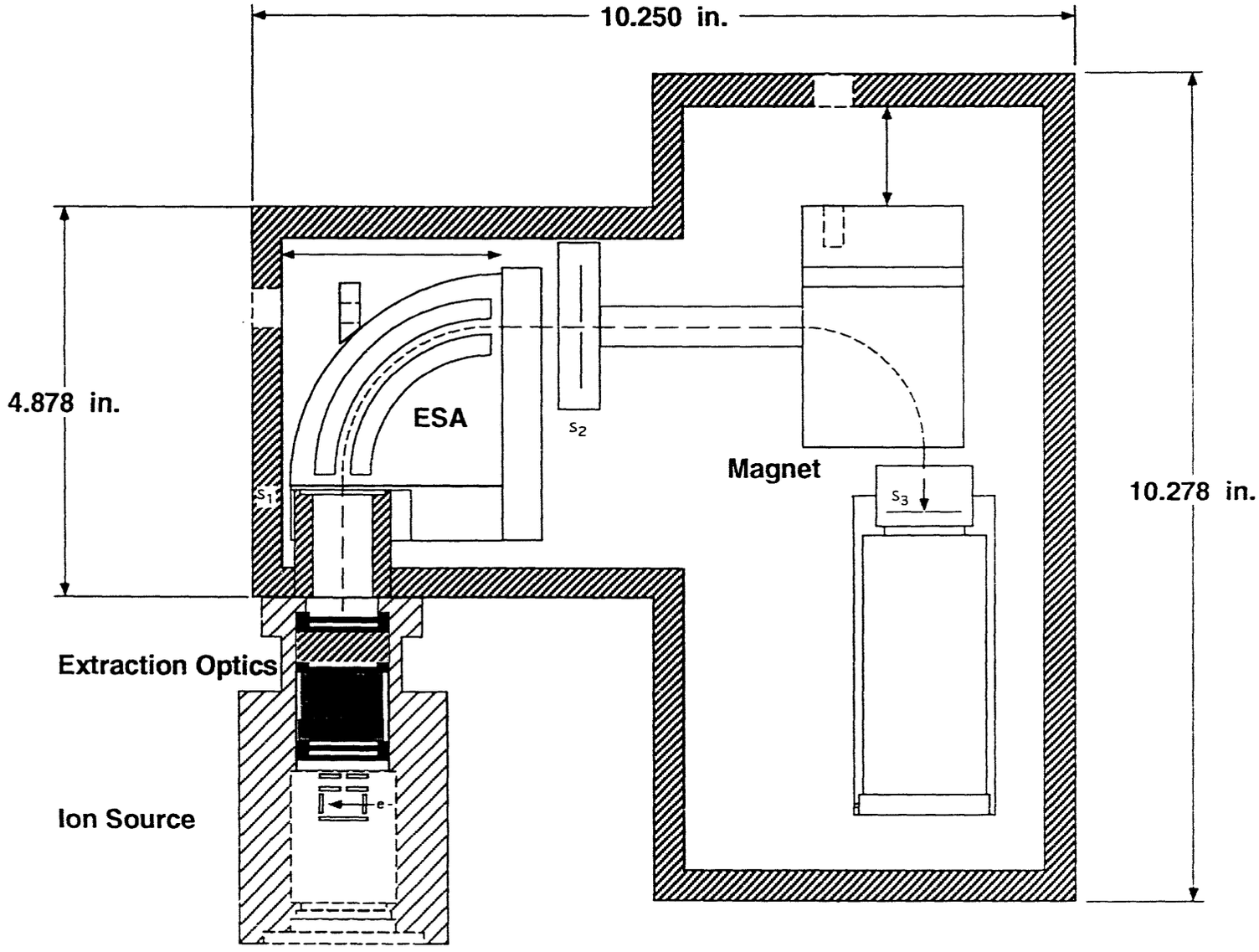

Dimension 1:1

Fig 2

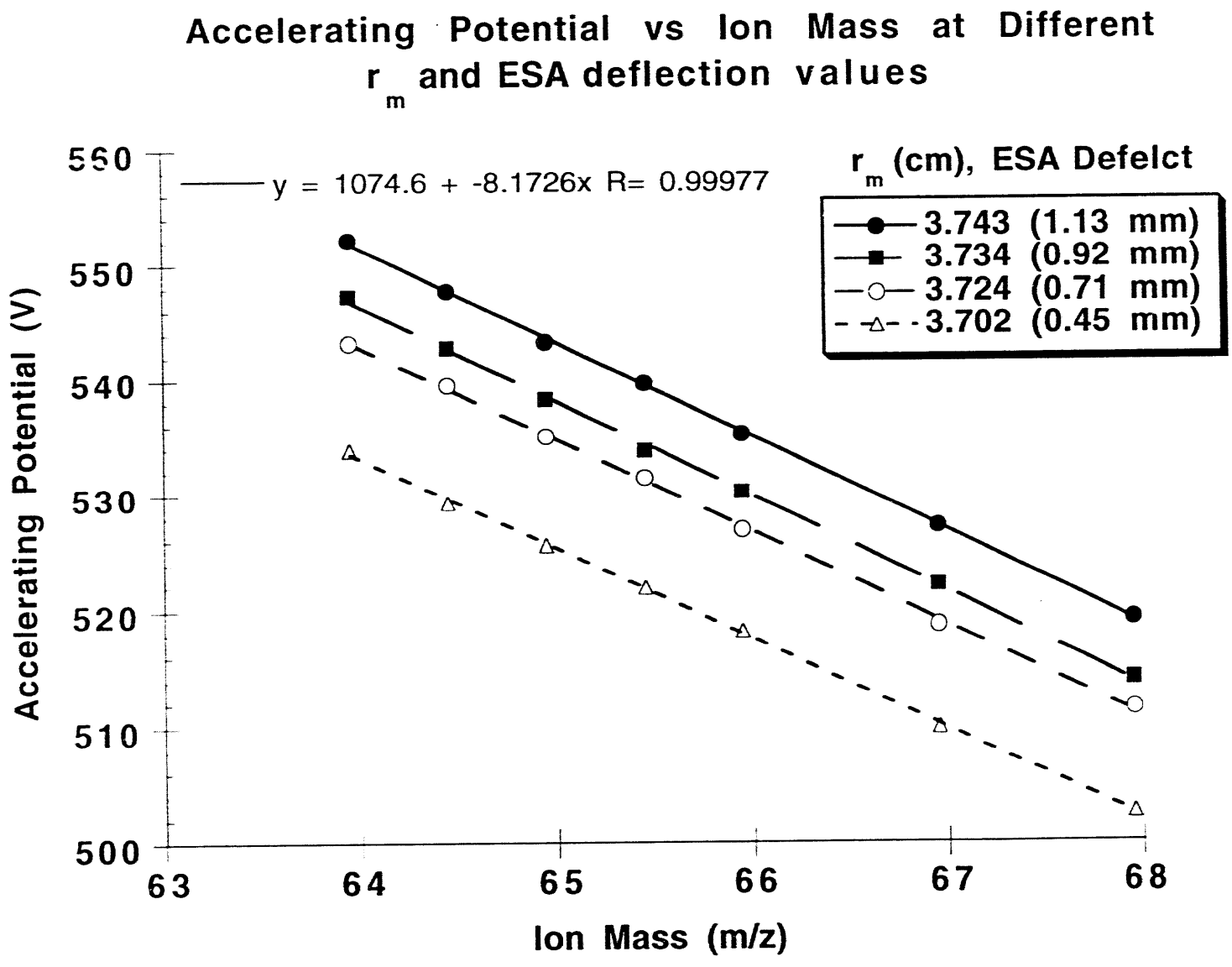
Accelerating Potential vs Ion Mass at Different r m and ESA deflection values
y = 1074.6 + -8.1726x R= 0.99977
r m (cm), ESA Defelct
3.743 (1.13 mm)
3.734 (0.92 mm)
3.724 (0.71 mm)
3.702 (0.45 mm)
Accelerating Potential (V)
560
550
540
530
520
510
500
63
64
65
66
67
68
Ion Mass (m/z)

Fig 2

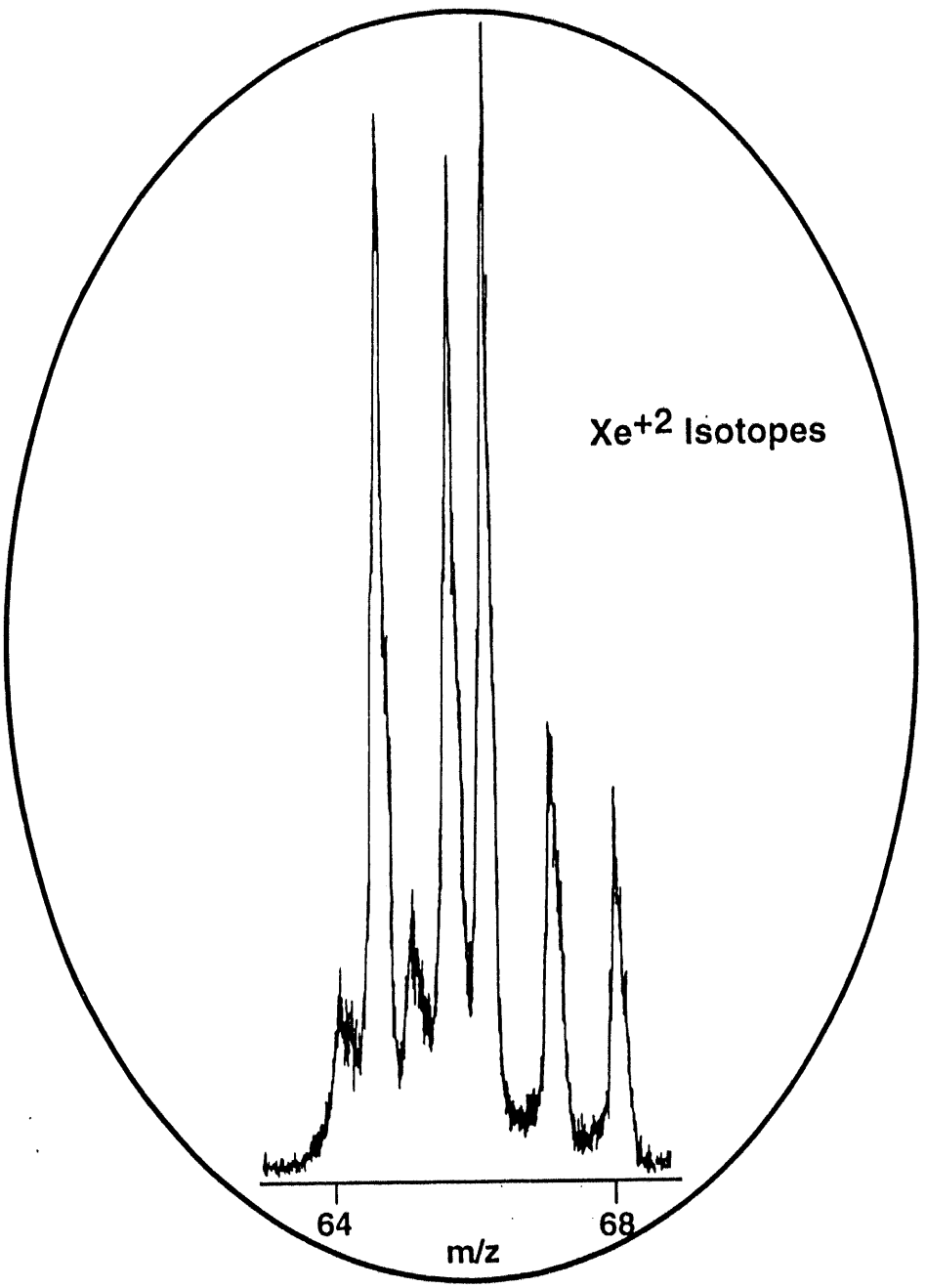

Fig 2

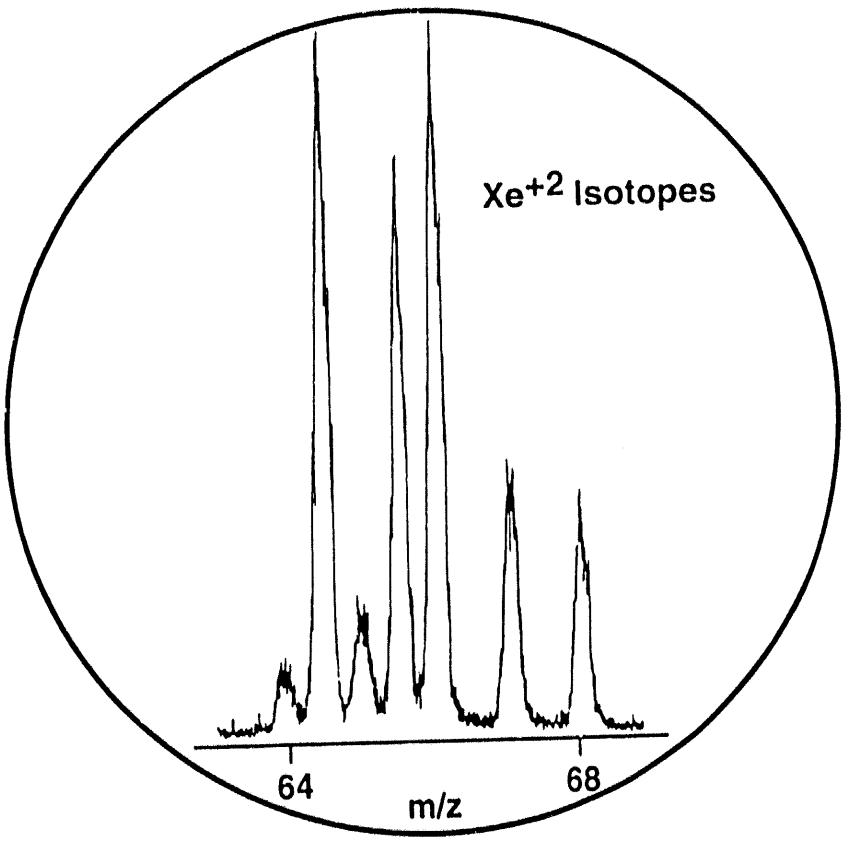

Fig 3

Magnetic Fringing Field Flux Density versus Distance

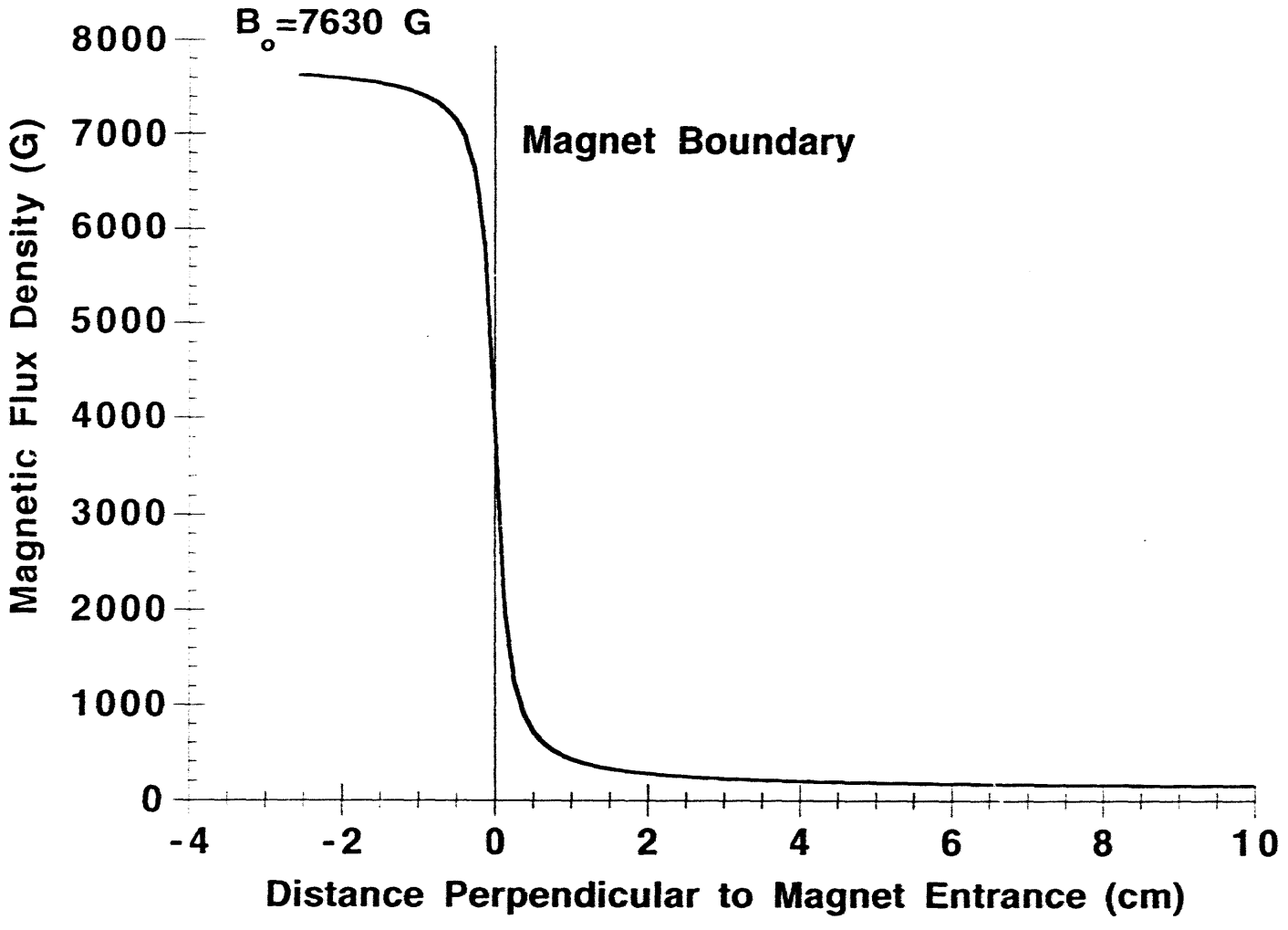

Ion Beam Focusing by Moving Magnet Position

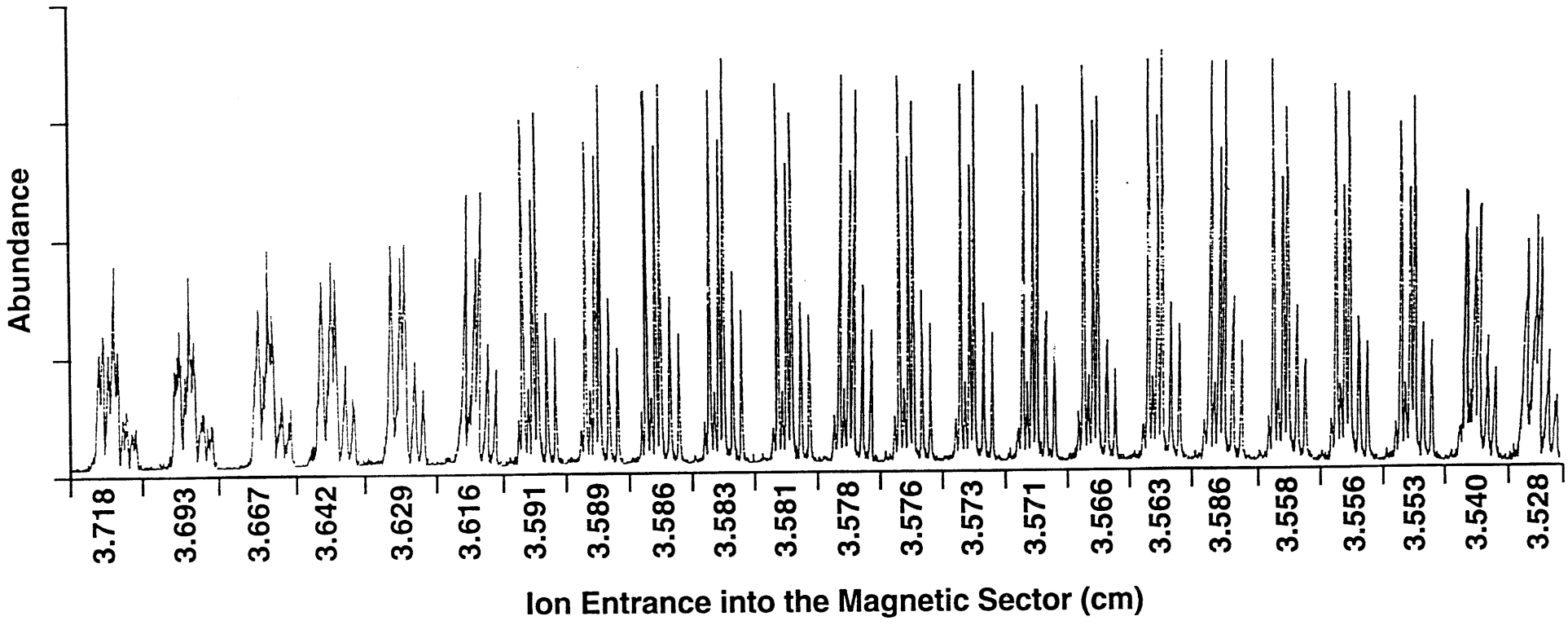

Fig 5

Entrance coordinate, **a**, has little effect on exit corrdinate, **h**, at an r_m

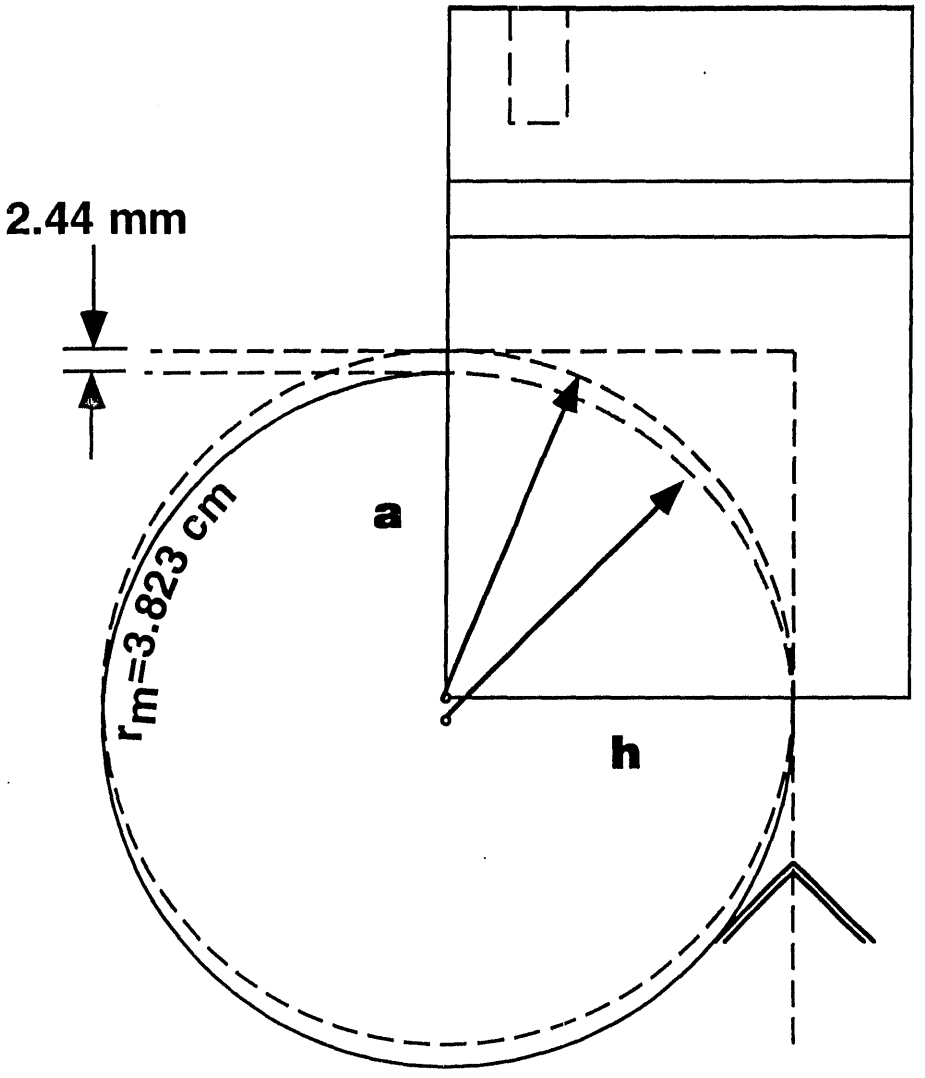

$$h = \sqrt{r_m \times 2\,a - a^2}$$

Fig 6

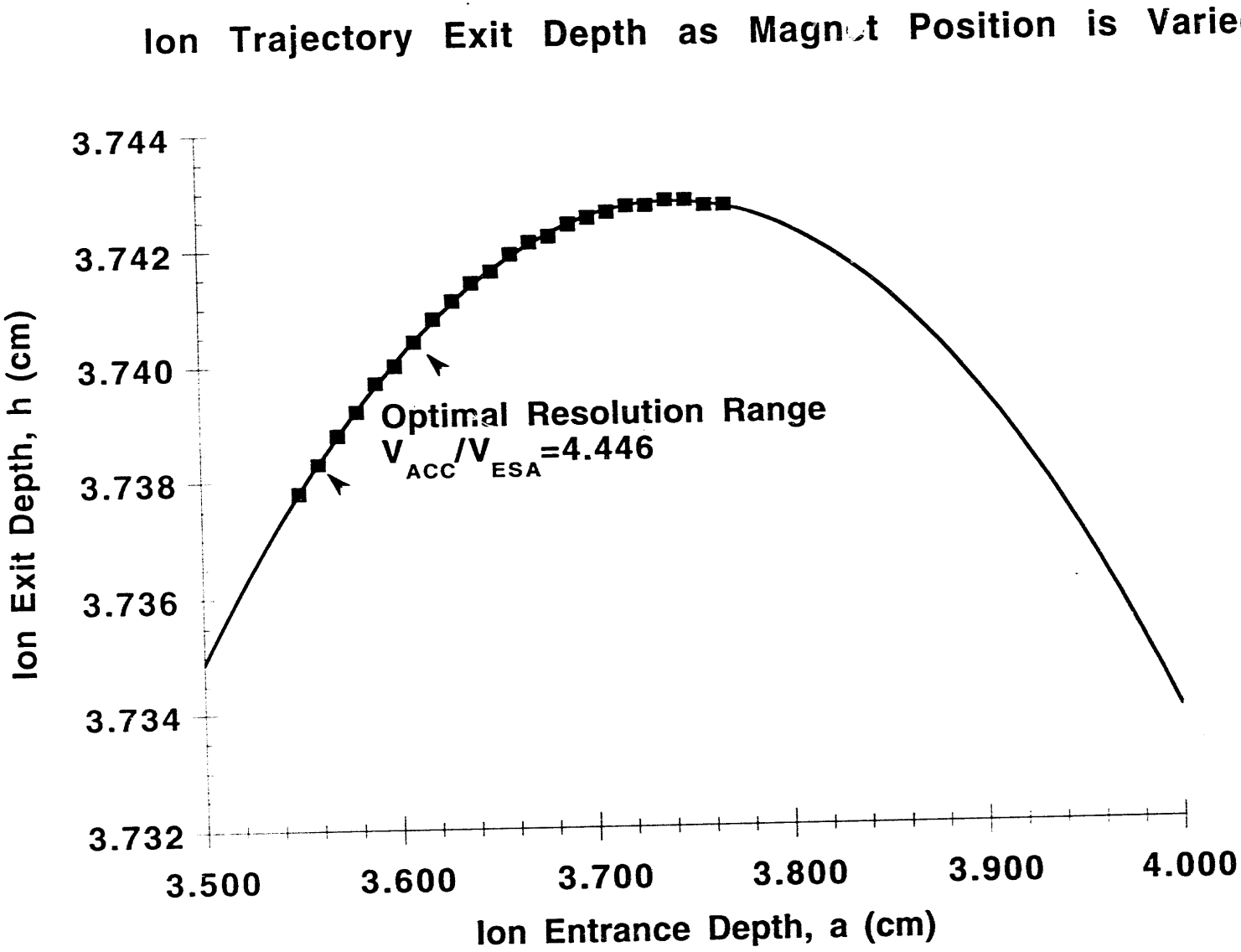
Ion Trajectory Exit Depth as Magnet Position is Varied
Ion Exit Depth, h (cm)
3.744
3.742
3.740
3.738
3.736
3.734
3.732
Optimal Resolution Range
V_ACC/V_ESA=4.446
3.500
3.600
3.700
3.800
3.900
4.000
Ion Entrance Depth, a (cm)

Fig 7

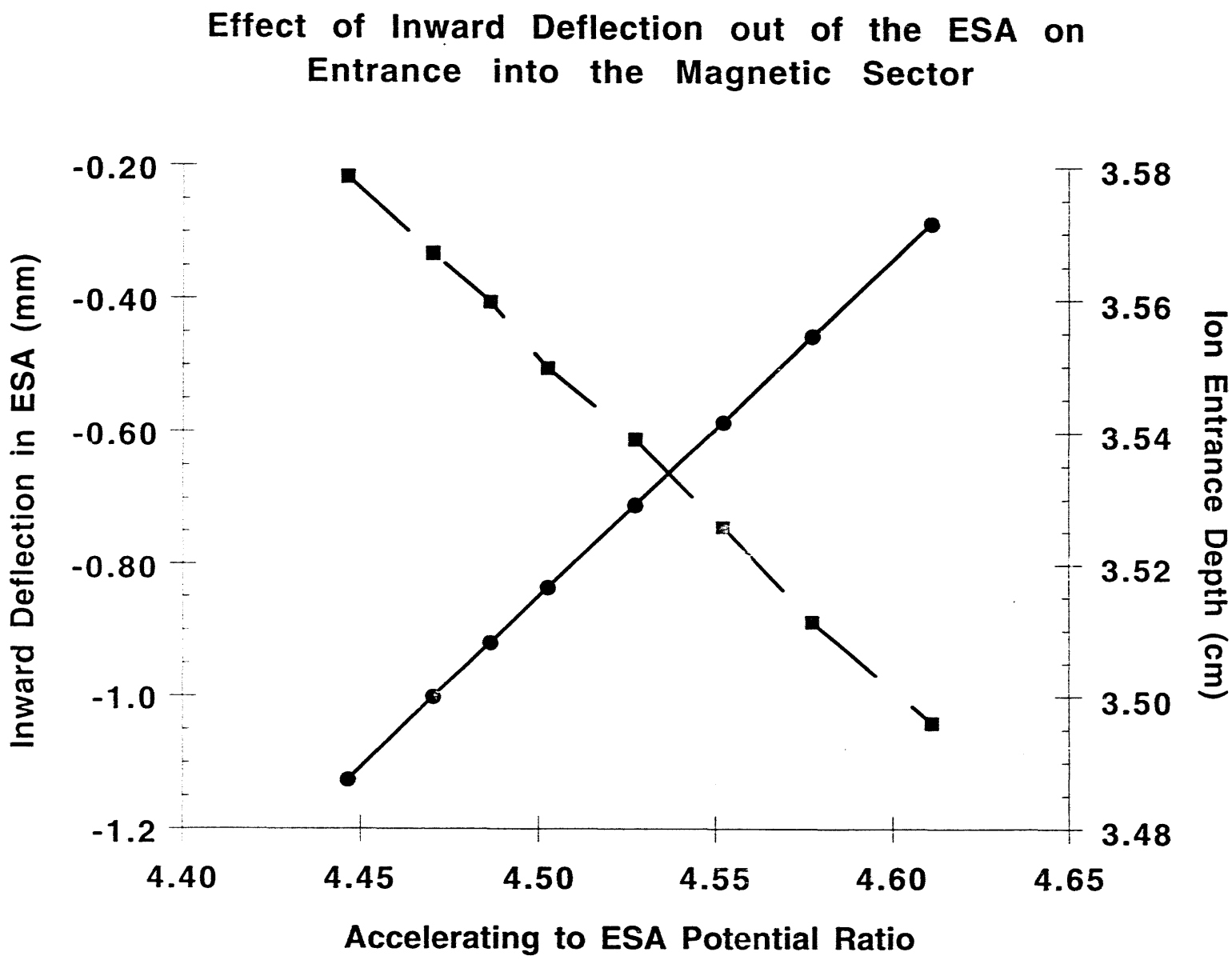
Effect of Inward Deflection out of the ESA on Entrance into the Magnetic Sector
Inward Deflection in ESA (mm)
-0.20
-0.40
-0.60
-0.80
-1.0
-1.2
Ion Entrance Depth (cm)
3.58
3.56
3.54
3.52
3.50
3.48
4.40
4.45
4.50
4.55
4.60
4.65
Accelerating to ESA Potential Ratio

DATE
FILMED
11/29/93
END